# Single-particle spectral function for the classical one-component plasma

C. Fortmann*
*Institut für Physik, Universität Rostock, 18051 Rostock, Germany*
(Received 15 August 2008; published 8 January 2009)

The spectral function for an electron one-component plasma is calculated self-consistently using the $GW^{(0)}$ approximation for the single-particle self-energy. In this way, correlation effects that go beyond the mean-field description of the plasma are contained, i.e., the collisional damping of single-particle states, the dynamical screening of the interaction, and the appearance of collective plasma modes. Second, a nonperturbative analytic solution for the on-shell $GW^{(0)}$ self-energy as a function of momentum is presented. It reproduces the numerical data for the spectral function with a relative error of less than 10% in the regime where the Debye screening parameter is smaller than the inverse Bohr radius, $\kappa < 1 a_B^{-1}$. In the limit of low density, the nonperturbative self-energy behaves as $n^{1/4}$, whereas a perturbation expansion leads to the unphysical result of a density-independent self-energy [Fennel and Wilfer, Ann. Phys. (Leipzig) **32**, 265 (1974)]. The derived expression will greatly facilitate the calculation of observables in correlated plasmas (transport properties, equation of state) that need the spectral function as an input quantity. This is demonstrated for the shift of the chemical potential, which is computed from the analytical formulas and compared to the $GW^{(0)}$ result. At a plasma temperature of 100 eV and densities below $10^{21}$ cm$^{-3}$, the two approaches deviate by less than 10% from each other.

DOI: 10.1103/PhysRevE.79.016404 PACS number(s): 52.27.Aj, 52.65.Vv, 71.15.−m

## I. INTRODUCTION

The many-particle Green function approach [1] allows for a systematic study of macroscopic properties of correlated systems. Green functions have a long history of applications in solid state theory [2], nuclear [3], and hadron physics [4], and also in the theory of strongly coupled plasmas [5]. In the last case, optical and dielectric properties [6,7] have been studied using the Green function approach, as well as transport properties like conductivity [8] and stopping power [9,10], and the equation of state [11]. Modifications of these quantities due to the interaction among the constituents can be accessed, starting from a common starting point, namely, the Hamiltonian of the system.

The key quantity for electronic properties in a correlated many-body environment is the electron spectral function $A(\mathbf{p},\omega)$, i.e., the probability density to find an electron at energy (frequency) $\omega$ for a given momentum $\mathbf{p}$. It is related to the retarded electron self-energy $\Sigma(\mathbf{p},\omega+i\delta), \delta>0$, via Dyson's equation

$$A(\mathbf{p},\omega) = \frac{-2\,\mathrm{Im}\,\Sigma(\mathbf{p},\omega+i\delta)}{[\omega-\varepsilon_{\mathbf{p}}-\mathrm{Re}\,\Sigma(\mathbf{p},\omega)]^2+[\mathrm{Im}\,\Sigma(\mathbf{p},\omega+i\delta)]^2}. \tag{1}$$

Here, the single-particle energy

$$\varepsilon_{\mathbf{p}} = p^2 - \mu_e \tag{2}$$

has been introduced, where $\mu_e$ is the electron chemical potential. Note that here and throughout the paper the Rydberg system of units is used, where $\hbar=1$, $m_e=1/2$, and $e^2/4\pi\epsilon_0=2$. Furthermore, the Boltzmann constant $k_B$ is set equal to 1, i.e., temperatures are measured in units of energy.

The self-energy describes the influence of correlations on the behavior of the electrons. A finite, frequency-dependent self-energy leads to a finite lifetime of single-particle states and a modification of the single-particle dispersion relation. Hence, the calculation of the electron self-energy is the central task if one wants to determine electronic properties, e.g., those mentioned above.

The Hartree-Fock approximation [12] represents the lowest order in a perturbative expansion of the self-energy in terms of the interaction potential [13]. Because it is a mean-field approximation, effects due to correlations in the system cannot be described. Examples are the appearance of collective modes, the energy transfer during particle collisions, and the quasiparticle damping. The next-order term is the Born approximation, where binary collisions are taken into account via a bare Coulomb potential. However, the Born approximation leads to a divergent integral, due to the long-range Coulomb interaction. Therefore, the perturbation expansion of the self-energy has to be replaced by a nonperturbative approach, accounting for the dynamical screening of the interparticle potential.

A nonperturbative approach to the many-particle problem is given by the theory of Dyson [14] and Schwinger [15,16] generalized to finite temperature and finite density [17]. An excellent introduction to the Dyson-Schwinger equations can also be found in [4]. The Dyson-Schwinger equation for the self-energy $\Sigma$ contains the full Green function $G$, the screened interaction $W$, and the proper vertex $\Gamma$. Since each of these functions obeys a different Dyson-Schwinger equation itself, involving higher-order correlation functions, the Dyson-Schwinger approach leads to a hierarchy of coupled integro-differential equations. In order to provide soluble equations, this hierarchy has to be closed at some level, i.e., correlation functions of a certain order have to be either parametrized or neglected.

One such closure of the Dyson-Schwinger hierarchy consists in neglecting the vertex, i.e., the three-point function, and considering only the particle propagators and their re-

*carsten.fortmann@uni-rostock.de;
http://everest.mpg.uni-rostock.de/~carsten

 

spective self-energies, i.e., two-point functions. One arrives at the so-called *GW* approximation, introduced in solid-state physics by Hedin [18]. Hedin was led by the idea of including correlations in the self-energy by replacing the Coulomb potential in the Hartree-Fock self-energy by the dynamically screened interaction $W$. In this way, one obtains a self-consistent, closed set of equations for the self-energy, the polarization function $\Pi$, the Green function, and the screened interaction.

It can be shown [19] that the *GW* approximation is one of the so-called $\Phi$-derivable approximations [20,21]. As such, it leads to energy-, momentum-, and particle-number-conserving expressions for higher-order correlation functions. It has been successfully applied in virtually all branches of solid state physics. An overview of theoretical foundations and applications of the *GW* approximation can be found in the review articles [22–24].

The drawback of the *GW* approximation is that the Ward-Takahashi identities are violated. The Ward-Takahashi identities provide an exact relation between the vertex function $\Gamma$, i.e., the effective electron-photon coupling in the medium, and the self-energy, and follow from the Dyson-Schwinger equations. They reflect the gauge invariance of the theory. In *GW* theory, they are violated simply because corrections to the vertex beyond zero order are neglected altogether. This issue touches on a fundamental problem in many-body theory and field theory, namely, the question of how to preserve gauge invariance in an effective, i.e., approximate, theory, without violating basic conservation laws. A detailed analysis of this question with application to nuclear physics is presented in a series of papers by van Hees and Knoll [25–27].

Approximations for the self-energy that also contain the vertex are often referred to as $GW\Gamma$ approximations. An example can be found in Ref. [28], where the spectral function of electrons in aluminum is calculated using a parametrized vertex function. An interesting result obtained in that work is that vertex corrections and self-energy corrections entering the polarization function largely cancel. This can be understood as a consequence of the Ward-Takahashi identities. Thus, and in order to reduce the numerical cost, it is a sensible choice to neglect vertex corrections altogether, and to keep the polarization function on the lowest level, i.e. the random phase approximation (RPA), which is the convolution product of two noninteracting Green functions in frequency-momentum space. The corresponding self-energy is named the $GW^{(0)}$ self-energy and has been introduced by von Barth and Holm [29], who were also the first to study the fully self-consistent *GW* approximation [30]. Throughout this work, the $GW^{(0)}$ self-energy will be analyzed.

Having been used in solid state physics traditionally, the $GW^{(0)}$ method was recently also applied to study correlations in hot and dense plasmas. The equation of state [31,32], as well as optical properties of electron-hole plasmas in highly excited semiconductors [33] and dense hydrogen plasmas [7] were investigated.

In general, the calculation of such macroscopic observables of many-particle system involves numerical operations that need the spectral function as an input. Since the self-consistent calculation of the self-energy, even in the $GW^{(0)}$ approximation, is itself already a numerically demanding task, it is worth looking for an analytic solution of the $GW^{(0)}$ equations which reproduces the numerical solution at least in a certain range of plasma parameters. Such an analytic expression then also allows study of the self-energy in various limiting cases, such as the low-density limit or the limit of high momenta, which are difficult to access in the numerical treatment. Furthermore, an analytic expression that is already close to the numerical solution permits the calculation of the full $GW^{(0)}$ self-energy using only few iterations.

Analytical expressions for the single-particle self-energy have already been given by other authors, e.g., Fennel and Wilfer [34] and Kraeft *et al.* [12]. They calculated the self-energy in first order of the perturbation expansion with respect to the dynamically screened potential. Besides being far from the converged $GW^{(0)}$ self-energy, their result is independent of density, i.e., the single-particle lifetime is finite even in vacuum. As shown in [35], this unphysical behavior is a direct consequence of the perturbative treatment. By using a nonperturbative ansatz, an expression for the self-consistent self-energy in a classical one-component plasma was presented that reproduces the full $GW^{(0)}$ self-energy at small momenta, i.e., for slow particles. The behavior of the quasiparticle damping at larger momenta remained open and will be investigated in the present work. Second, based on the information gathered about the low- and high-momentum behavior, an interpolation formula will be derived that gives the quasiparticle damping at arbitrary momenta.

The work is organized in the following way. After a brief outline of the $GW^{(0)}$ approximation in the next section, numerical results will be given in Sec. III for the single-particle spectral function for various sets of parameters, electron density $n$, and electron temperature $T$. In Sec. IV the analytic expression for the quasiparticle damping width is presented and comparison to the numerical results is given. Section V deals with the application of the derived formulas to the calculation of the chemical potential as a function of density and temperature. An Appendix contains the detailed derivation of the analytic self-energy. As a model system, we focus on the electron one-component plasma; ions are treated as a homogeneously distributed background of positive charges (jellium model).

## II. SPECTRAL FUNCTION AND SELF-ENERGY

We start our discussion with the integral equation for the imaginary part of the single-particle self-energy in the $GW^{(0)}$ approximation:

$$\mathrm{Im}\,\Sigma(\mathbf{p},\omega+\mathrm{i}\delta)=\frac{1}{n_{\mathrm{F}}(\omega)}\sum_{\mathbf{q}}\int_{-\infty}^{\infty}\frac{\mathrm{d}\omega'}{2\pi}V(q)A(\mathbf{p}-\mathbf{q},\omega-\omega')\times\mathrm{Im}\,\epsilon_{\mathrm{RPA}}^{-1}(\mathbf{q},\omega')n_{\mathrm{B}}(\omega')n_{\mathrm{F}}(\omega-\omega'). \quad (3)$$

$V(q)=8\pi/q^2\Omega_0$ is the Fourier transform of the Coulomb potential with the normalization volume $\Omega_0$. It is multiplied by the inverse dielectric function in the RPA,

$$\epsilon_{\mathrm{RPA}}(q,\omega) = 1 - V(q)\sum_{\mathbf{p}} \frac{n_{\mathrm{F}}(\varepsilon_{\mathbf{p}-\mathbf{q}/2}) - n_{\mathrm{F}}(\varepsilon_{\mathbf{p}+\mathbf{q}/2})}{\omega + \varepsilon_{\mathbf{p}-\mathbf{q}/2} - \varepsilon_{\mathbf{p}+\mathbf{q}/2}}, \quad (4)$$

to account for dynamical screening of the interaction. Furthermore, the Fermi-Dirac and the Bose-Einstein distribution functions, $n_{\mathrm{F/B}}(\varepsilon)=[\exp(\varepsilon/k_{\mathrm{B}}T)\pm 1]^{-1}$ were introduced. Note that the dielectric function is determined only once, at the beginning of the calculation. In particular, the single-particle energies $\varepsilon_{\mathbf{p}}=p^2-\mu_{\mathrm{e}}$ entering Eq. (4) are determined from the noninteracting chemical potential, whereas during the course of the self-consistent calculation of the self-energy, the chemical potential is recalculated at each step via inversion of the density relation

$$n(\mu_e,T) = 2\sum_{\mathbf{p}} \int \frac{d\omega}{2\pi} A(\mathbf{p},\omega) n_{\mathrm{F}}(\omega). \quad (5)$$

Using the self-consistent chemical potential also in the RPA polarization function leads to violation of the $f$-sum rule, i.e., conservation of the number of particles.

The real part of the self-energy is obtained via the Kramers-Kronig relation [2]. All quantities (spectral function, self-energy, and chemical potential) have to be determined in a self-consistent way. This is usually achieved by solving Eqs. (1)–(3) iteratively. The numerical algorithm is discussed in detail in Ref. [35].

## III. NUMERICAL RESULTS

The spectral function was calculated for the case of a hot one-component electron plasma. Temperature and density were chosen such that the plasma degeneracy parameter

$$\theta = \frac{T}{E_{\mathrm{F}}} \quad (6)$$

is always larger than 1, i.e., the plasma is nondegenerate. Furthermore, the temperature is fixed above the ionization energy of hydrogen, $T \gg 1$ Ry, such that bound states can be neglected in the calculations. At lower temperatures, bound states have to be included, e.g., via the $t$ matrix. For an application in electron-hole plasmas, see Ref. [33]. The electron density is adjusted such that the plasma coupling parameter

$$\Gamma = \frac{2}{T}\left(\frac{4\pi n}{3}\right)^{1/3}, \quad (7)$$

which gives the mean Coulomb interaction energy compared to the thermal energy, is smaller than 1 in all calculations, i.e., we are in the limit of weak coupling.

In Fig. 1, we show contour plots of the spectral function in frequency and momentum space for two different densities $n=7\times10^{21}$ cm$^{-3}$ (upper graph) and $7\times10^{25}$ cm$^{-3}$ (lower graph). The temperature is set to $T=1000$ eV in both calculations. The free particle dispersion $\omega=\varepsilon_p$ is shown as a solid black line.

In the first case, the plasma is classical ($\theta=7.5\times10^2$) and weakly coupled ($\Gamma=4.4\times10^{-3}$). The spectral function is symmetrically broadened and the maximum is found at the free dispersion, i.e., there is no notable quasiparticle shift in the present conditions. With increasing momentum, the width of the spectral function decreases, and the maximum value increases; the norm is preserved.

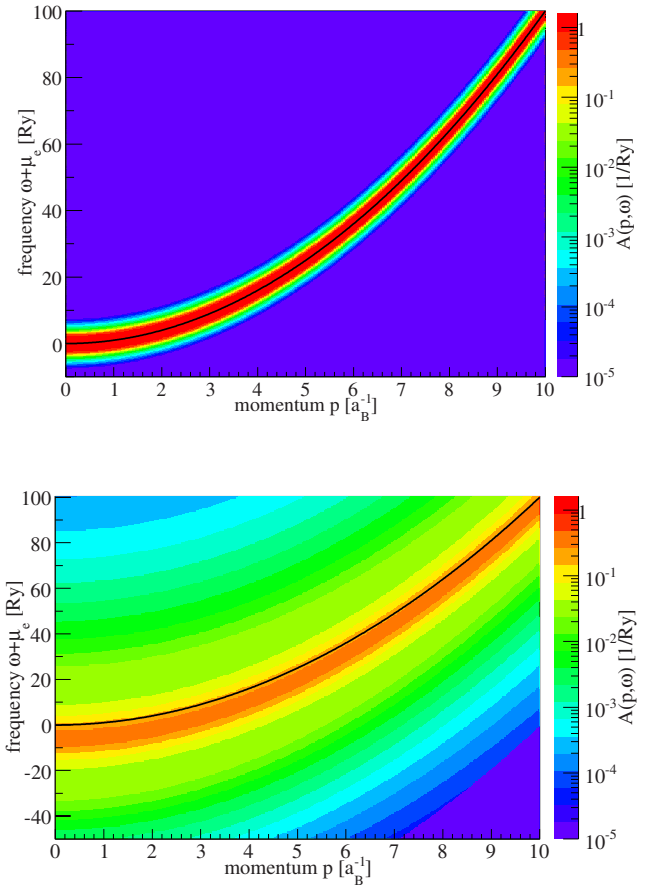


FIG. 1. (Color online) Contour plots of the spectral function as a function of momentum and frequency. The color scale is logarithmic. Results are shown for two different densities $n=7\times10^{21}$ (upper graph) and $7\times10^{25}$ cm$^{-3}$ (lower graph). For these parameters, the plasma coupling parameter is $\Gamma=4.4\times10^{-3}$ and $9.6\times10^{-2}$, respectively. The degeneracy parameter is $\theta=7.5\times10^2$ and 1.6, respectively. The black line indicates the free particle dispersion $\omega=\varepsilon_p$.

The situation changes when we go to higher densities (see the lower graph in Fig. 1). The chosen parameters are typical solar core parameters [36]. The degeneracy parameter is now $\theta=1.6$ and the coupling parameter is $\Gamma=0.096$. The increased degeneracy and coupling result in a significant modification of the spectral function as compared to the low-density case: A shift of the spectral function's maximum to smaller frequencies is observed, the Hartree-Fock shift. The shift due to dynamic correlations is still small in the present conditions; it becomes important in strongly degenerate systems [29]. Furthermore, shoulders appearing in the wings of the main quasiparticle peak at small momenta indicate the excitation of new quasiparticles, so-called plasmarons [37]. They can be seen more clearly in Fig. 7 (solid curve). The plasmaron satellites are separated from the main peak by roughly the plasma frequency $\omega_{\mathrm{pl}}=4\sqrt{\pi n}$, which is about 23 Ry at the present density. In the former case of lower density no plas-

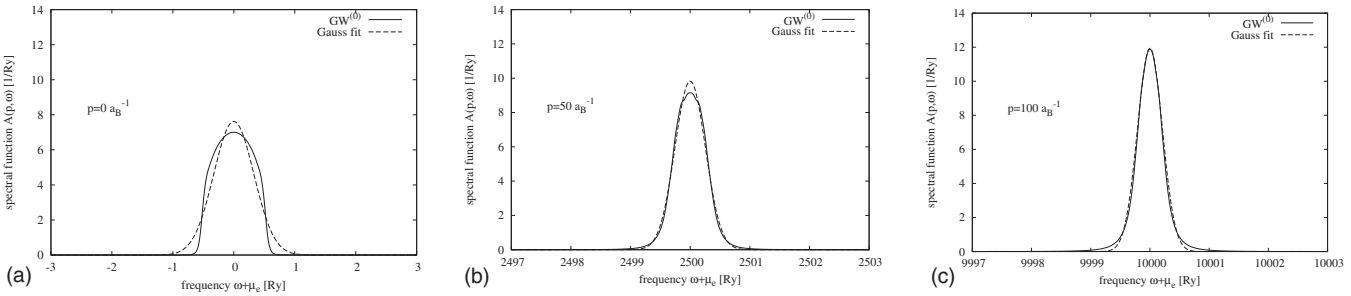


FIG. 2. Spectral function in $GW^{(0)}$-approximation (solid lines) and Gaussian ansatz (dashed lines) with quasiparticle damping width $\sigma_p$ taken from Eq. (17) for three different momenta $p=$(a) 0, (b) $50a_B^{-1}$, and (c) $100a_B^{-1}$. Plasma parameters: $n=7\times10^{19}$ cm$^{-3}$, $T=100$ eV. The plasma coupling parameter is $\Gamma=1.0\times10^{-2}$, the degeneracy parameter is $\theta=1.6\times10^{3}$, and the Debye screening parameter is $\kappa=6.0\times10^{-3}a_B^{-1}$.

marons appear; only a featureless, single resonance is obtained. At higher momenta, the plasmarons merge into the central peak. As in the low-density case, the position of the maximum approaches the single-particle dispersion, due to the decreasing Hartree-Fock shift at high $p$. Again, the width of the spectral function decreases with increasing momentum.

This is visible more clearly in Figs. 2–7. Here, the solid curves represent the $GW^{(0)}$ spectral function as a function of frequency. Results are shown for three different momenta, $p=0a_B^{-1}$ (a), $50a_B^{-1}$ (b), and $100a_B^{-1}$ (c). Two different temperatures are considered, $T=100$ (Figs. 2–4) and 1000 eV (Figs. 5–7), and for each temperature three different densities are studied. With increasing momentum $p$, the spectral function becomes more and more narrow, converging eventually into a narrow on-shell resonance, located at the unperturbed single-particle dispersion $\omega+\mu_e=p^2$.

As a general feature, one can observe an increase of the spectral function's width with increasing density and with increasing temperature. The increase with density is due to the increased coupling, while the increase with temperature reflects the thermal broadening of the momentum distribution function $n_F(\omega)$ that enters the self-energy and thereby also the spectral function. From these results, we see that the spectral function has a quite simple form in the limit of low coupling, i.e., at low densities and high temperatures.

The numerical results are compared to a Gaussian ansatz for the spectral function, shown as the dashed curve in Figs. 2–7. The explicit form of the Gaussian is given as Eq. (11), below. Its sole free parameter is the width, denoted by $\sigma_p$. An analytic expression for $\sigma_p$ will be derived in Sec. IV. The coincidence is in general good at high momenta, whereas at low momenta the spectral function deviates from the Gaussian. In particular, the steep wings and the smoother plateau that form at low momenta are not reproduced by the Gaussian. Also, the plasmaron peaks appearing in the spectral function at high density (see Fig. 7) cannot be described by the single Gaussian.

Determination of $\sigma_p$ via least-squares fitting of the Gaussian ansatz to the numerical data at each $p$ leads to the solid curve in Fig. 8, obtained in the case of $n=7\times10^{20}$ cm$^{-3}$ and $T=100$ eV. Starting at some finite value $\sigma_0$ at $p=0$, the width falls off slowly toward larger $p$. The dashed curve shows $\sigma_p$ as obtained from the analytic formula that will be derived in the following section.

## IV. ANALYTICAL EXPRESSION FOR THE QUASI-PARTICLE SELF-ENERGY

The solution of the $GW^{(0)}$ equation (3) requires a considerable numerical effort. So far (see, e.g. the work by Fennel and Wilfer in [34]), attempts to solve the integral (3) analytically were led by the idea of replacing the spectral function on the right-hand side (RHS) by its noninteracting counterpart, $A^{(0)}(\mathbf{p},\omega)=2\pi\delta(\varepsilon_{\mathbf{p}}-\omega)$, i.e., going back to the perturbation expansion of the self-energy and neglecting the implied self-consistency. At the same time, the inverse dielectric function is usually replaced by a simplified expres-

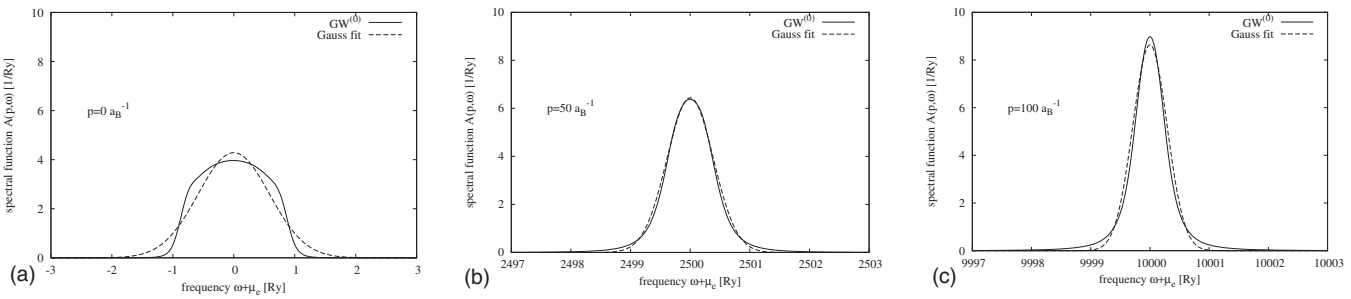


FIG. 3. Spectral function in $GW^{(0)}$ approximation (solid lines) and Gaussian ansatz (dashed lines) with quasiparticle damping width $\sigma_p$ taken from Eq. (17) for three different momenta $p=$(a) 0, (b) $50a_B^{-1}$, and (c) $100a_B^{-1}$. Plasma parameters: $n=7\times10^{20}$ cm$^{-3}$, $T=100$ eV. The plasma coupling parameter is $\Gamma=2.1\times10^{-2}$, the degeneracy parameter is $\theta=3.5\times10^{2}$, and the Debye screening parameter is $\kappa=1.9\times10^{-2}a_B^{-1}$.

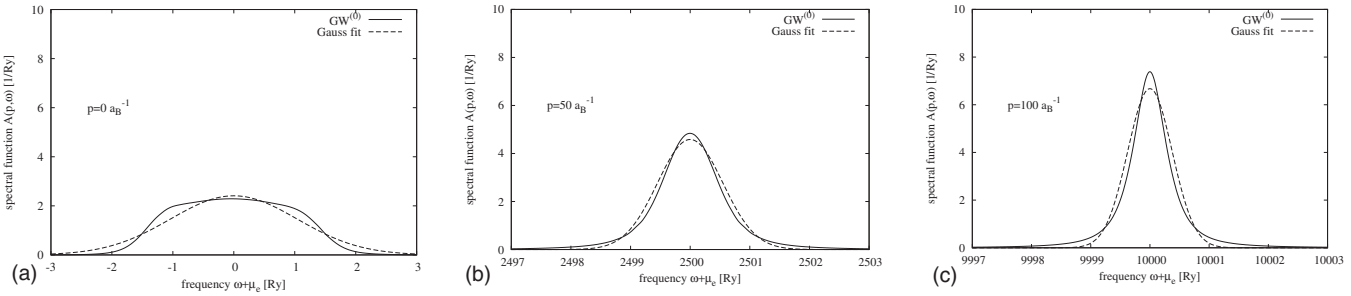


FIG. 4. Spectral function in $GW^{(0)}$ approximation (solid lines) and Gaussian ansatz (dashed lines) with quasiparticle damping width $\sigma_p$ taken from Eq. (17) for three different momenta $p=$(a) 0, (b) $50a_B^{-1}$, and (c) $100a_B^{-1}$. Plasma parameters: $n=7\times10^{21}$ cm$^{-3}$, $T=100$ eV. The plasma coupling parameter is $\Gamma=4.4\times10^{-2}$, the degeneracy parameter is $\theta=7.5\times10^{1}$, and the Debye screening parameter is $\kappa=6.0\times10^{-2}a_B^{-1}$.

sion, e.g., the Born approximation or the plasmon-pole approximation [12]. Whereas the second simplification is indispensable due to the complicated structure of the inverse dielectric function, the first one, i.e., the recursion to the quasiparticle picture, is not necessary, as was shown by the author in Ref. [35]. In fact, the result that one obtains in the quasiparticle approximation is far from the converged result, at least in the high-temperature case. Second, if the quasiparticle approximation is used, the imaginary part of the self-energy is not density dependent, i.e., a finite lifetime of the particle states is obtained even in vacuum. This unphysical result can be overcome only if one sticks to the self-consistency of the self-energy, i.e., if one leaves the imaginary part of the self-energy entering the RHS of Eq. (3) finite.

Using the statically screened Born approximation, which describes the binary collisions among electrons via a statically screened potential, a scaling law $\mathrm{Im}\,\Sigma(\mathbf{p},\omega^{\mathrm{QP}}(\mathbf{p}))\propto\Gamma^{3/4}$ was found [35]. Hence, the spectral function width vanishes when the plasma coupling parameter $\Gamma$ [see Eq. (7)] tends to 0. An expression for the self-energy was found that reproduces the converged $GW^{(0)}$ calculations at small momenta, $p\ll\kappa$. At higher momenta, the derived expression ceases to be valid.

In this work, a different approximation to the dielectric function is studied, namely, the plasmon-pole approximation [12]. This means that the inverse dielectric function is replaced by a sum of two $\delta$ functions that describe the location of the plasmon resonances,

$$\mathrm{Im}\,\epsilon^{-1}_{\mathrm{RPA}}(\mathbf{q},\omega')\rightarrow\mathrm{Im}\,\epsilon^{-1}_{\mathrm{PPA}}(\mathbf{q},\omega')$$
$$=-\frac{\pi}{2}\frac{\omega_{\mathrm{pl}}^2}{\omega_{\mathbf{q}}}[\delta(\omega-\omega_{\mathbf{q}})+\delta(\omega+\omega_{\mathbf{q}})]. \quad (8)$$

For classical plasmas, the plasmon dispersion $\omega_{\mathbf{q}}$ can be approximated by the Bohm-Gross dispersion relation [38]

$$\omega_{\mathbf{q}}^2=\omega_{\mathrm{pl}}^2\left(1+\frac{q^2}{\kappa^2}\right)+q^4. \quad (9)$$

Many-particle and quantum effects on the plasmon dispersion have recently been studied in [39].

The plasmon-pole approximation (PPA) allows one to perform the frequency integration in Eq. (3), resulting in the expression

$$\mathrm{Im}\,\Sigma(\mathbf{p},\omega+i\delta)=\frac{\omega_{\mathrm{pl}}^2}{4}\sum_{\mathbf{q}}V(q)\frac{1}{\omega_{\mathbf{q}}}[A(\mathbf{p}-\mathbf{q},\omega-\omega_{\mathbf{q}})$$
$$\times n_{\mathrm{B}}(\omega_{\mathbf{q}})\exp(\omega_{\mathbf{q}}/T)-A(\mathbf{p}-\mathbf{q},\omega+\omega_{\mathbf{q}})$$
$$\times n_{\mathrm{B}}(-\omega_{\mathbf{q}})\exp(-\omega_{\mathbf{q}}/T)]. \quad (10)$$

We will first study the case of high momenta, i.e., momenta that are large against any other momentum scale or inverse length scale, such as the mean momentum with respect to the Boltzmann distribution, $\bar{p}=\sqrt{3T/2}$, or the inverse screening length $\kappa=\sqrt{8\pi n/T}$.

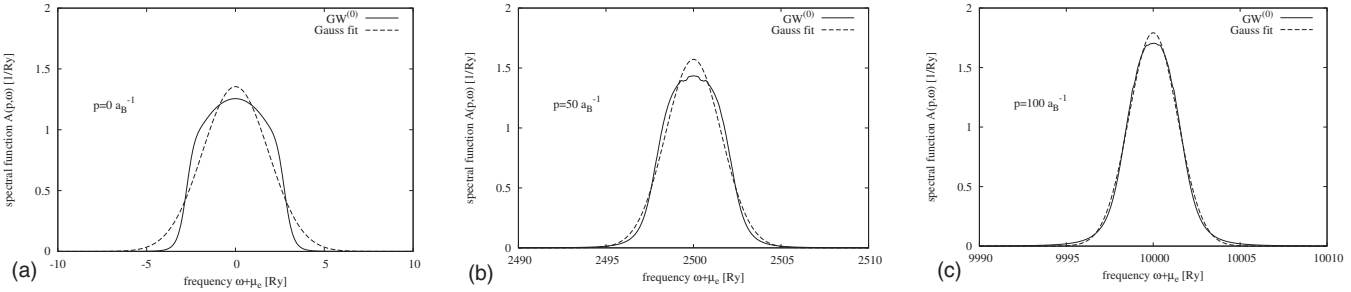


FIG. 5. Spectral function in $GW^{(0)}$ approximation (solid lines) and Gaussian ansatz (dashed lines) with quasiparticle damping width $\sigma_p$ taken from Eq. (17) for three different momenta $p=$(a) 0, (b) $50a_B^{-1}$, and (c) $100a_B^{-1}$. Plasma parameters: $n=7\times10^{21}$ cm$^{-3}$, $T=1000$ eV. The plasma coupling parameter is $\Gamma=4.4\times10^{-3}$, the degeneracy parameter is $\theta=7.5\times10^{2}$, and the Debye screening parameter is $\kappa=1.9\times10^{-2}a_B^{-1}$.

As discussed in the previous section, the numerical results for the spectral function at high momenta can well be reproduced by a Gaussian. Thus, we make the following ansatz for the spectral function:

$$A_{\mathrm{Gauss}}(\mathbf{p},\omega) = -\frac{\sqrt{2\pi}}{\sigma_p}\exp\left(-\frac{[\omega-\varepsilon_{\mathbf{p}}-\Sigma^{\mathrm{HF}}(\mathbf{p})]^2}{2\sigma_p^2}\right). \quad (11)$$

Note that only the Hartree-Fock contribution to the real part of the self-energy appears. The frequency-dependent part is usually small near the quasiparticle dispersion,

$$\omega^{\mathrm{QP}}(\mathbf{p}) = \varepsilon_{\mathbf{p}} + \mathrm{Re}\,\Sigma(\mathbf{p},\omega)\,|_{\omega=\omega^{\mathrm{QP}}(\mathbf{p})}, \quad (12)$$

which therefore can be approximated as $\omega^{\mathrm{QP}}(\mathbf{p})=\varepsilon_{\mathbf{p}}+\mathrm{Re}\,\Sigma^{\mathrm{HF}}(\mathbf{p})$. In the following, we make use of the knowledge about the width parameter $\sigma_p$ that we gathered already through simple least-squares fitting of the Gaussian ansatz to the spectral function in order to solve the integrals in Eq. (10).

First, we replace the spectral function on the RHS by the Gaussian ansatz (11) and evaluate the emerging equation at the single-particle dispersion $\omega^{\mathrm{QP}}(\mathbf{p})$. By claiming that the Gaussian and the spectral function have the same value at the quasiparticle energy, we identify $\sigma_p=\sqrt{\pi/2}\mathrm{Im}\,\Sigma(\mathbf{p},\omega^{\mathrm{QP}}(\mathbf{p}))$. Figure 8 shows that the quasiparticle damping $\sigma_p$ is a smooth function of $p$ that varies only little on the scale of the screening parameter $\kappa$. Since the latter defines the scale on which contributions to the $q$ integral are most important, we can neglect the momentum shift in the self-energy on the RHS, i.e., we can replace the spectral function on the RHS of Eq. (10) by

$$A(\mathbf{p}-\mathbf{q},\varepsilon_{\mathbf{p}}+\Sigma^{\mathrm{HF}}(\mathbf{p})\pm\omega_{\mathbf{q}}) \to -\frac{\sqrt{2\pi}}{\sigma_p}\exp\left(-\frac{(\varepsilon_{\mathbf{p}}\pm\omega_{\mathbf{q}}-\varepsilon_{\mathbf{p}-\mathbf{q}})^2}{2\sigma_p^2}\right), \quad (13)$$

and can now perform the integral over the angle $\theta$ between the momenta $\mathbf{p}$ and $\mathbf{q}$,

$$\frac{\sqrt{2\pi}}{\sigma_p}\int_{-1}^{1} d\cos\theta \times\exp\left(-\frac{(\varepsilon_{\mathbf{p}}\pm\omega_{\mathbf{q}}-p^2-q^2+2pq\cos\theta+\mu_e)^2}{2\sigma_p^2}\right) = \frac{\pi}{2pq}\left[\mathrm{Erf}\left(\frac{(p+q)^2-p^2\mp\omega_{\mathbf{q}}}{\sqrt{2}\sigma_p}\right) - \mathrm{Erf}\left(\frac{(p-q)^2-p^2\pm\omega_{\mathbf{q}}}{\sqrt{2}\sigma_p}\right)\right]. \quad (14)$$

The remaining integration over the modulus of the transfer momentum $q$ can be performed after some further approximations, explained in detail in Appendix A. For large $p$, one finally obtains the transcendental equation

$$\sigma_p = -1.3357\sqrt{\frac{\pi}{2}}\frac{\omega_{\mathrm{pl}}}{2p}[n_{\mathrm{B}}(\omega_{\mathrm{pl}})\exp(\omega_{\mathrm{pl}}/T) - n_{\mathrm{B}}(-\omega_{\mathrm{pl}})\exp(-\omega_{\mathrm{pl}}/T)] - \sqrt{\frac{\pi}{2}}\frac{T}{2p}\ln(\kappa^2p^2/\sigma_p^2). \quad (15)$$

The solution of this equation can be expanded for large arguments of the logarithm, yielding

$$\sigma_p = -\sqrt{\frac{\pi}{2}}\frac{T}{p}\varphi(p),$$

$$\varphi(p) = \left(\xi(p) - \ln\xi(p) + \frac{\ln\xi(p)}{\xi(p)} - \frac{\ln\xi(p)}{\xi^2(p)} + \frac{\ln\xi(p)}{\xi(p)} - \frac{3\ln^2\xi(p)}{2\xi^3(p)} + \frac{\ln^2\xi(p)}{2\xi^2(p)} + \frac{\ln^3\xi(p)}{3\xi^3(p)}\right) + O(p)^{-3},$$

$$\xi(p) = \ln\left(\sqrt{\frac{2}{\pi}}\kappa p^2\exp(A/T)/T\right), \quad (16)$$

$$A = -1.3357\frac{\omega_{\mathrm{pl}}}{2}[n_{\mathrm{B}}(\omega_{\mathrm{pl}})\exp(\omega_{\mathrm{pl}}/T) - n_{\mathrm{B}}(-\omega_{\mathrm{pl}})\exp(-\omega_{\mathrm{pl}}/T)].$$

Equation (16) is a solution of Eq. (15) provided the argument of the inner logarithm is larger than Euler's constant $e$, i.e., $\sqrt{2/\pi}\kappa p^2\exp(A/T)/T>e$, i.e., at large $p$. The case of small $p$, where the previous inequality does not hold, has to be treated separately; see Appendix B.

Together with an expression for the quasiparticle damping at vanishing momentum taken from [35] and scaled such that the maximum of the spectral function at $p=0$ is reproduced, $\sigma_0=-\pi\sqrt{\kappa T}/2$, an interpolation formula (Padé formula) was derived that covers the complete $p$ range:

$$\sigma_p^{\mathrm{Padé}} = \frac{a_0+a_1p}{1+b_1p+b_2p^2}\tilde{\varphi}(p),$$

$$\tilde{\varphi}(p) = \left(\tilde{\xi}(p) - \ln\tilde{\xi}(p) + \frac{\ln\tilde{\xi}(p)}{\tilde{\xi}(p)} - \frac{\ln\tilde{\xi}(p)}{\tilde{\xi}^2(p)} + \frac{\ln\tilde{\xi}(p)}{\tilde{\xi}(p)} - \frac{3\ln^2\tilde{\xi}(p)}{2\tilde{\xi}^3(p)} + \frac{\ln^2\tilde{\xi}(p)}{2\tilde{\xi}^2(p)} + \frac{\ln^3\tilde{\xi}(p)}{3\tilde{\xi}^3(p)}\right),$$

$$\tilde{\xi}(p) = \ln\left(e + \sqrt{\frac{2}{\pi}}\kappa p^2\exp(A/T)/T\right),$$

$$a_0 = -\frac{\pi}{2}\sqrt{\kappa T}, \quad a_1 = -\kappa\left(\frac{\pi}{2}\right)^{3/2}, \quad b_1 = \sqrt{\frac{\pi\kappa}{2T}}, \quad b_2 = \frac{\pi\kappa}{2T}. \quad (17)$$

The function $\tilde{\xi}(p)$ in the last equation differs from $\xi(p)$ in Eq. (16) in that Euler's constant $e\simeq 2.7183$ has been added to the

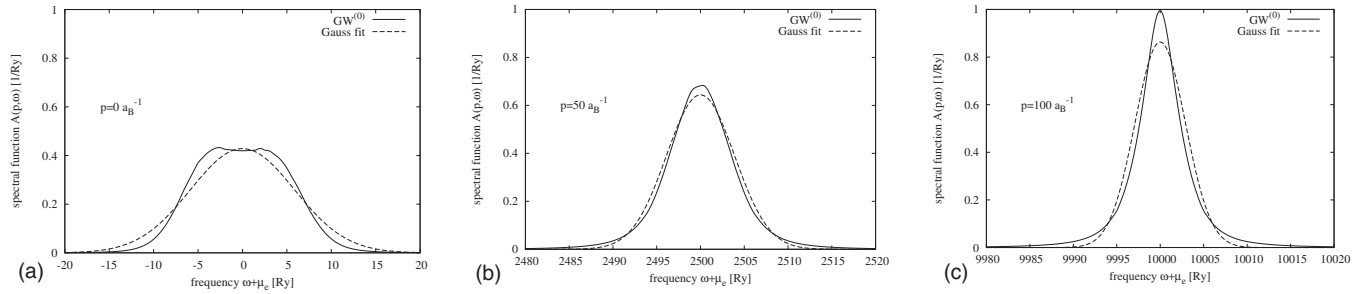


FIG. 6. Spectral function in $GW^{(0)}$ approximation (solid lines) and Gaussian ansatz (dashed lines) with quasiparticle damping width $\sigma_p$ taken from Eq. (17) for three different momenta $p$=(a) 0, (b) $50a_B^{-1}$, and (c) $100a_B^{-1}$. Plasma parameters: $n=7\times10^{23}$ cm$^{-3}$, $T=1000$ eV. The plasma coupling parameter is $\Gamma=2.1\times10^{-2}$, the degeneracy parameter is $\theta=3.5\times10^{1}$, and the Debye screening parameter is $\kappa=1.9\times10^{-1}a_B^{-1}$.

argument of the logarithm. In this way, the function $\tilde{\varphi}(p)$ is regularized at small $p$ and tends to 1 at $p=0$, i.e., the quasiparticle damping goes to the correct low-$p$ limit. At large $p$, this modification is insignificant, since the original argument rises as $p^2$. For the detailed derivation, see Appendix B.

Expression (17), used in the Gaussian ansatz (11), leads to a spectral function that well reproduces the numerical data from full $GW^{(0)}$ calculations: Figure 8 (dashed curve) shows the effective quasiparticle damping width $\sigma_p$ as a function of momentum $p$ for the case $n=7\times10^{20}$ cm$^{-3}$ and $T=100$ eV. The solid curve gives the best-fit value for $\sigma_p$ obtained via least-squares fitting of the full $GW^{(0)}$ calculations assuming the Gaussian form (11) (see Sec. III). The two curves coincide to a large extent. The largest deviations are observed in the range of $p\simeq20a_B^{-1}$. At this point, the validity of expression (16) as the solution of Eq. (15) ceases, since the argument of the logarithm becomes smaller than $e$. As already mentioned, we circumvented this problem by regularizing the logarithm, adding $e$ to its argument. The deviation at $p\simeq20a_B^{-1}$ of up to 15% is a residue of this procedure. At higher momenta, the deviation is generally smaller than 10% and the analytic formula evolves parallel to the fit parameters.

At smaller densities, the correspondence is even better as can be seen by comparing the spectral functions shown in Figs. 2–7. The dashed curves give the Gaussian ansatz for the spectral function with the quasiparticle width taken from the interpolation formula (17). As a general result, the analytic expression for the quasiparticle damping $\sigma_p$ leads to a spectral function that nicely fits the numerical solution for the spectral function at least at finite $p$. At very small values of $p$, the overall correspondence is still fair, i.e., the position of the maximum and the overall width match, but the detailed behavior does not coincide. In particular, the steep wings and the central plateau that form in the $GW^{(0)}$ calculation are not reproduced by the one-parameter Gaussian. For this situation, the analytic formula for self-energy given in [35] should be used instead.

By comparing the numerical data for the spectral function to the Gaussian ansatz at different densities, it is found that the Gaussian spectral function is a good approximation as long as the Debye screening parameter $\kappa$ is smaller than the inverse Bohr radius, $\kappa<1a_B^{-1}$. This becomes obvious by comparing Figs. 6 and 7. In the first case ($n=7\times10^{23}$ cm$^{-3}$, $T=1000$ eV), we have $\kappa=0.19$, while in the second case ($n=7\times10^{25}$ cm$^{-3}$, $T=1000$ eV), $\kappa=1.9$ is found. As already noted in the discussion of the numerical results in Sec. III, in the case of increased density, the plasmaron satellites appear as separate structures in the wings of the central quasiparticle peak, whereas they are hidden in the central peak at smaller densities. Therefore, a single Gaussian is not sufficient to fit the spectral function at increased densities. Since the position of the plasmaron peak is given approximately by the plasma frequency $\omega_{pl}$, whereas the width of the central peak at small $p$ is just the quasiparticle width $\sigma_0$, we can identify the ratio of these two quantities, $-\omega_{pl}/\sigma_0\propto\sqrt{\kappa}$, as the parameter that

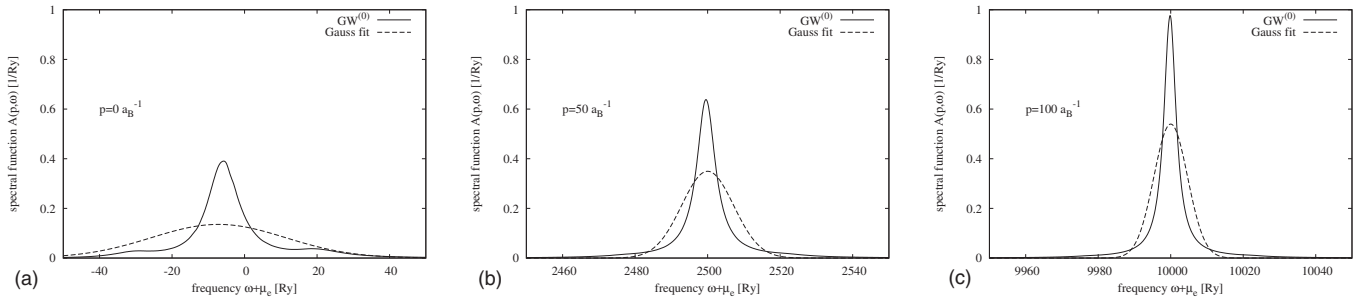


FIG. 7. Spectral function in $GW^{(0)}$ approximation (solid lines) and Gaussian ansatz (dashed lines) with quasiparticle damping width $\sigma_p$ taken from Eq. (17) for three different momenta $p$=(a) 0, (b) $50a_B^{-1}$, and (c) $100a_B^{-1}$. Plasma parameters: $n=7\times10^{25}$ cm$^{-3}$, $T=1000$ eV. The plasma coupling parameter is $\Gamma=9.6\times10^{-2}$, the degeneracy parameter is $\theta=1.6$, and the Debye screening parameter is $\kappa=1.9a_B^{-1}$. Here, the Gaussian fit is no longer sufficient due to the appearance of plasmaron resonances in the spectral function (shoulders at $\omega\simeq-30$ and $\simeq20$ Ry).

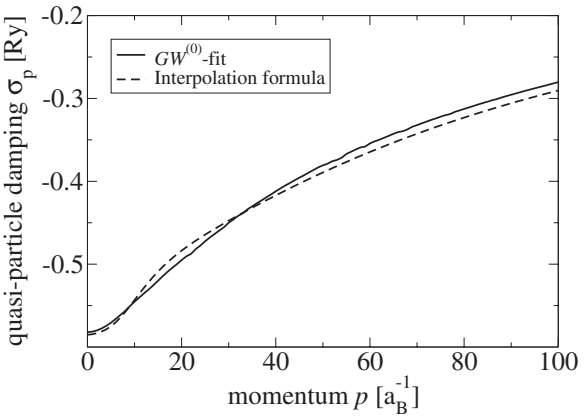


FIG. 8. Effective quasiparticle damping $\sigma_p$ as a function of momentum $p$ for plasma density $n=7\times10^{20}$ cm$^{-3}$ and temperature $T=100$ eV. The fit parameters for the Gaussian fit to the full $GW^{(0)}$ calculations are given as the solid line; the dashed line denotes the analytic interpolation formula (17).

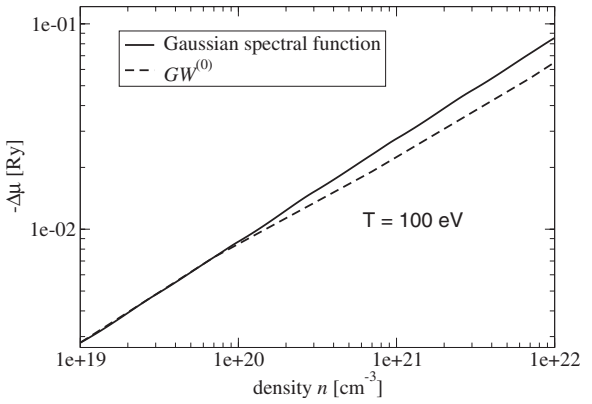


FIG. 9. Shift of the chemical potential as a function of the plasma density for a plasma temperature $T=100$ eV. Results for $\Delta\mu$ using the parametrized spectral function (solid line) are compared to full numerical calculations, using the $GW^{(0)}$ approximation (dashed line).

tells us if plasmaron peaks appear separately ($\omega_{\rm pl}>-\sigma_0$) or not ($\omega_{\rm pl}<-\sigma_0$). Since the plasma frequency increases as a function of $n^{1/2}$, whereas the quasiparticle width scales as $n^{1/4}$ [see Eq. (17)], the transition from the single-peak behavior to the more complex behavior including plasmaron resonances appears at increased density. Neglecting numerical constants of order 1 in the ratio of plasma frequency to damping width, we see that $-\omega_{\rm pl}/\sigma_0<1$ is equivalent to $\kappa<1$, which was our observation from the numerical results. Therefore, we can identify the range of validity of the presented expressions for the spectral function and the quasiparticle damping. It is valid for those plasmas where we have densities and temperatures such that $\kappa<1$.

The physical origin of the requirement $\kappa<1$ can be understood in the following way [35]. At length scales smaller than the Bohr radius, one typically expects quantum effects, e.g., Pauli blocking. These effects are not accounted for in the derivation of the quasiparticle damping. Therefore, it appears to be a logical consequence that the validity of the results is limited by the length scale at which typical quantum phenomena become important.

The regime of validity of the analytic formula can also be expressed via the plasma coupling parameter and the temperature as $\Gamma<T^{-2/3}$. Since we restrict ourselves to plasma temperatures where bound states can be excluded, i.e., $T>1$ Ry, this is equivalent to saying that $\Gamma<1$.

Although the correspondence between the accurate $GW^{(0)}$ calculations and the parametrized spectral function at small momenta is not as good as in the case of large momenta, the parametrized spectral function can be applied in the regime of validity to the calculation of plasma observables without introducing too large errors. As an example, this will be shown for the case of the chemical potential $\mu$ in the next section.

## V. APPLICATION: SHIFT OF THE CHEMICAL POTENTIAL

To demonstrate the applicability of the presented formulas for quick and reliable calculations of plasma properties, we calculate the shift of the electron's chemical potential $\Delta\mu=\mu-\mu_{\rm free}$, i.e., the deviation of the chemical potential of the interacting plasma $\mu$ from the value of the noninteracting system $\mu_{\rm free}$. The chemical potential of the interacting system $\mu$ is obtained by inversion of the density as a function of $T$ and $\mu$, Eq. (5). The free chemical potential $\mu_{\rm free}$ is obtained in a similar way by inversion of the free density,

$$n_{\rm free}(T,\mu_{\rm free})=2\sum_{\mathbf{p}} n_{\rm F}(\varepsilon_{\mathbf{p}}-\mu_{\rm free}). \tag{18}$$

Figure 9 shows the shift of the chemical potential as a function of the plasma density $n$ for a fixed plasma temperature $T=100$ eV. Results obtained by inversion of Eq. (5) using the parametrized spectral function (11) with the quasiparticle damping width taken from Eq. (17) (solid curve) are compared to those results taking the numerical $GW^{(0)}$ spectral function (dashed curve).

The $GW^{(0)}$ result gives slightly smaller shifts than the parametrized spectral function, i.e., the usage of the analytical damping width leads to an overestimation of the shift of the chemical potential. However, the deviation remains smaller than 20% over the range of densities considered here, i.e., for $\kappa<1$. At small densities, i.e., for $n\leqslant10^{20}$ cm$^{-3}$, the parametrized spectral function yields the same result as the full $GW^{(0)}$ calculation.

The deviation at increased density can be reduced by improving the parametrization of the spectral function at small momenta. To this end, the behavior of the quasiparticle damping width at high momenta, Eq. (16) should be combined with the frequency-dependent solution for $\sigma_p$ at vanishing momentum, as presented in Ref. [35]. However, this task goes beyond the scope of this paper, where we wish to present comparatively simple analytic expressions for the damping width that yield the correct low-density behavior of plasma properties.

## VI. CONCLUSIONS AND OUTLOOK

In this paper, the $GW^{(0)}$ approximation for the single-particle self-energy was evaluated for the case of a classical

one-component electron plasma, with ions treated as a homogeneous charge background. A systematic behavior of the spectral function was found, i.e., a symmetrically broadened structure at low momenta and convergence to a sharp quasiparticle resonance at high $p$. At increased densities, plasmaron satellites show up in the spectral function as satellites besides the main peak.

In the second part, an analytic formula for the imaginary part of the self-energy at the quasiparticle dispersion $\omega^{\mathrm{QP}}(\mathbf{p})=\varepsilon_{\mathbf{p}}+\Sigma^{\mathrm{HF}}(\mathbf{p})$ was derived as a two-point Padé formula that interpolates between the exactly known behavior at $p=0$ and $p\to\infty$. The former case was studied in [35], while an expression for the asymptotic case $p\to\infty$ was derived here. The result is summarized in Eq. (17). In contrast to previously known expressions for the quasiparticle damping, based on a perturbative approach to the self-energy [34], the result presented here shows a physically intuitive behavior in the limit of low densities, i.e., it vanishes when the system becomes dilute. Use of the Gaussian ansatz (11) for the spectral function in combination with the quasiparticle width leads to a very good agreement with the numerical data for the spectral function in the range of plasma parameters where $\kappa<1a_{\mathrm{B}}^{-1}$; the relative deviation is smaller than 10% under this constraint.

Thus, a simple expression for the damping width of electrons in a classical plasma has been found, which can be used to approximate the full spectral function to high accuracy. This achievement greatly facilitates the calculation of observables that take the spectral function or the self-energy as an input, such as optical properties (inverse bremsstrahlung absorption), conductivity, or the stopping power.

Furthermore, it was demonstrated that the derived expressions allow for quick and reliable calculations of plasma properties without having to resort to the full self-consistent solution of the $GW^{(0)}$ approximation. As an example, the shift of the chemical potential was calculated using the parametrized spectral function, and compared to $GW^{(0)}$ results. For densities of $n<10^{21}$ cm$^{-3}$, the two approaches coincide with a relative deviation of less than 10%, going eventually up to 20% as the density approaches $10^{22}$ cm$^{-3}$. At low densities both approaches give identical results. This shows the extreme usefulness of the presented approach for the calculation of observables via the parametrized spectral function.

As a further important application of the results presented in this paper, we would like to mention the calculation of radiative energy loss of particles traversing a dense medium, i.e., bremsstrahlung. A many-body theoretical approach to this scenario is given by Knoll and Voskresensky [40], using nonequilibrium Green functions. They showed that a finite spectral width of the emitting particles leads to a decrease in the bremsstrahlung emission. This effect is known as the Landau-Pomeranchuk-Migdal effect [41,42]. It has been experimentally confirmed in relativistic electron scattering experiments using dense targets, e.g., lead [43,44]. In [45], it is shown that thermal bremsstrahlung from a plasma is also reduced due to the finite spectral width of the electrons in the plasma. In the cited papers, the quasiparticle damping width was either set as a momentum- and energy-independent parameter (in [40]), or calculated self-consistently using simplified approximations of the $GW^{(0)}$ theory (in [45]), which itself is a very time-consuming task and prohibited investigations over a broad range of plasmas parameters. Now, based on this work's results, calculations on the level of the full $GW^{(0)}$ approximation become feasible, since analytic formulas have been found that reproduce the $GW^{(0)}$ self-energy. Effects of dynamical correlations on the bremsstrahlung spectrum can be studied starting from a consistent single-particle description via the $GW^{(0)}$ self-energy.

## ACKNOWLEDGMENTS

The author acknowledges much helpful advice from Gerd Röpke and fruitful discussion with W.-D. Kraeft as well as with C. D. Roberts. Financial support was obtained from the German Research Society (DFG) via the Collaborative Research Center "Strong Correlations and Collective Effects in Radiation Fields: Coulomb Systems, Clusters, and Particles" (SFB 652).

## APPENDIX A: ANALYTIC SOLUTION FOR THE $GW^{(0)}$ SELF-ENERGY USING THE PLASMON-POLE APPROXIMATION

After the angular integration which was performed in Eq. (14), the imaginary part of the self-energy at the quasiparticle dispersion $\omega=\varepsilon_{\mathbf{p}}$ reads

$$\mathrm{Im}\,\Sigma(\mathbf{p},p^2)=\frac{\omega_{\mathrm{pl}}^2}{4p}\int_0^\infty\frac{dq}{q\omega_{\mathbf{q}}}\left\{\left[\mathrm{Erf}\left(\frac{q^2+2pq+\omega_{\mathbf{q}}}{\sqrt{2}\sigma_p}\right)-\mathrm{Erf}\left(\frac{q^2-2pq+\omega_{\mathbf{q}}}{\sqrt{2}\sigma_p}\right)\right]n_{\mathrm{B}}(\omega_{\mathbf{q}})\exp(\omega_{\mathbf{q}}/T)-\left[\mathrm{Erf}\left(\frac{q^2+2pq-\omega_{\mathbf{q}}}{\sqrt{2}\sigma_p}\right)-\mathrm{Erf}\left(\frac{q^2-2pq-\omega_{\mathbf{q}}}{\sqrt{2}\sigma_p}\right)\right]n_{\mathrm{B}}(-\omega_{\mathbf{q}})\exp(-\omega_{\mathbf{q}}/T)\right\}. \tag{A1}$$

This equation represents a self-consistent equation for $\mathrm{Im}\,\Sigma(\mathbf{p},\omega=p^2)=\sqrt{2/\pi}\sigma_p$.

Our aim is to derive an analytic expression that approximates the numerical solution of Eq. (A1) for arbitrary $p$. To this end, we first look at the case of large momenta, $p\gg\kappa$, and later combine that result with known expressions for the limit of vanishing momentum $p\to0$, to produce an interpolation ("Padé") formula that covers the complete $p$ range.

We perform a sequence of approximations to the integral in (A1). First, we observe, that at large $p$, the term $2pq$ dominates in the argument of the error function. We rewrite Eq. (A1) as

$$\sigma_p=\sqrt{\frac{\pi}{2}}\,\mathrm{Im}\,\Sigma(\mathbf{p},p^2)=\sqrt{\frac{\pi}{2}}\frac{\omega_{\mathrm{pl}}^2}{4p}\int_0^\infty\frac{dq}{q\omega_{\mathbf{q}}}\left\{\left[\mathrm{Erf}\left(\frac{2pq}{\sqrt{2}\sigma_p}\right)-\mathrm{Erf}\left(\frac{-2pq}{\sqrt{2}\sigma_p}\right)\right]n_{\mathrm{B}}(\omega_{\mathbf{q}})\exp(\omega_{\mathbf{q}}/T)-\left[\mathrm{Erf}\left(\frac{2pq}{\sqrt{2}\sigma_p}\right)-\mathrm{Erf}\left(\frac{-2pq}{\sqrt{2}\sigma_p}\right)\right]n_{\mathrm{B}}(-\omega_{\mathbf{q}})\exp(-\omega_{\mathbf{q}}/T)\right\} \tag{A2}$$

$$= \sqrt{\frac{\pi}{2}}\frac{\omega_{\rm pl}^2}{4p}\int_0^\infty \frac{dq}{q\omega_{\mathbf{q}}} 2\,\mathrm{Erf}\left(\frac{2pq}{\sqrt{2}\sigma_p}\right)[n_{\rm B}(\omega_{\mathbf{q}})\exp(\omega_{\mathbf{q}}/T) - n_{\rm B}(-\omega_{\mathbf{q}})\exp(-\omega_{\mathbf{q}}/T)]. \quad \text{(A3)}$$

The integrand in Eq. (A3) contains a steeply rising part at $q<-\sigma_p/p$ and a smoothly decaying part for at large $q$, i.e., when $q\gg-\sigma_p/p$. Therefore, we separate the integral in the equation into two parts, one going from $q=0$ to $q=\bar{q}=-\sigma_p/p$ and the other from $\bar{q}$ to infinity. In the first part of the integral, the values for $q$ are so small that we can replace the plasmon dispersion by the plasma frequency $\omega_{\rm pl}$. In the second term, the argument of the error function is large and the error function can be replaced by its asymptotic value at infinity, $\lim_{x\to\infty}\mathrm{Erf}(x)=1$. This leads to

$$\sigma_p = \sqrt{\frac{\pi}{2}}\frac{\omega_{\rm pl}^2}{4p}\left[\int_0^{\bar{q}} \frac{dq}{q\omega_{\rm pl}} 2\,\mathrm{Erf}\left(\frac{2pq}{\sqrt{2}\sigma_p}\right)[n_{\rm B}(\omega_{\rm pl})\exp(\omega_{\rm pl}/T) - n_{\rm B}(-\omega_{\rm pl})\exp(-\omega_{\rm pl}/T)] + 2\int_{\bar{q}}^\infty \frac{dq}{q\omega_{\mathbf{q}}}[n_{\rm B}(\omega_{\mathbf{q}})\exp(\omega_{\mathbf{q}}/T) - n_{\rm B}(-\omega_{\mathbf{q}})\exp(-\omega_{\mathbf{q}}/T)]\right]. \quad \text{(A4)}$$

Finally, we expand the last term in powers of $\omega_{\mathbf{q}}/T$, which is justified at low densities ($\omega_{\mathbf{q}}\propto\omega_{\rm pl}$), and keep only the first order,

$$n_{\rm B}(\omega_{\mathbf{q}})\exp(\omega_{\mathbf{q}}/T) - n_{\rm B}(-\omega_{\mathbf{q}})\exp(-\omega_{\mathbf{q}}/T) = \frac{2T}{\omega_{\mathbf{q}}} + O(\omega_{\mathbf{q}})^{-3}. \quad \text{(A5)}$$

We obtain

$$\sigma_p = \sqrt{\frac{\pi}{2}}\frac{\omega_{\rm pl}^2}{4p}\left[\int_0^{\bar{q}} \frac{dq}{q\omega_{\rm pl}} 2\,\mathrm{Erf}\left(\frac{2pq}{\sqrt{2}\sigma_p}\right)[n_{\rm B}(\omega_{\rm pl})\exp(\omega_{\rm pl}/T) - n_{\rm B}(-\omega_{\rm pl})\exp(-\omega_{\rm pl}/T)] + 4T\int_{\bar{q}}^\infty \frac{dq}{q\omega_{\mathbf{q}}^2}\right]. \quad \text{(A6)}$$

Both integrals can be performed analytically:

$$\begin{aligned}\int_0^{\bar{q}} \frac{dq}{q}\,\mathrm{Erf}\left(\frac{2pq}{\sqrt{2}\sigma_p}\right) &= -2\sqrt{\frac{2}{\pi}}\frac{p\bar{q}}{\sigma_p}\,{}_2F_2(1/2,1/2;3/2,3/2; -2p^2\bar{q}^2/\sigma_p^2)\\ &= -2\sqrt{\frac{2}{\pi}}\,{}_2F_2(1/2,1/2;3/2,3/2;-2)\\ &= -1.3357,\end{aligned}$$

$$\int_{\bar{q}}^\infty \frac{dq}{q\omega_{\rm pl}^2(1+q^2/\kappa^2)} = \frac{1}{2}\ln(1+\kappa^2/\bar{q}^2) = \frac{1}{2}\ln(1+\kappa^2p^2/\sigma_p^2), \quad \text{(A7)}$$

where $\bar{q}=-\sigma_p/p$ was used. Note that, in the second integral, the $q^4$ term in the plasmon dispersion (9) is omitted. ${}_2F_2(a_1,a_2;b_1,b_2;z)$ is the generalized hypergeometric function [46].

We arrive at the equation

$$\sigma_p = -1.3357\sqrt{\frac{\pi}{2}}\frac{\omega_{\rm pl}^2}{2p}[n_{\rm B}(\omega_{\rm pl})\exp(\omega_{\rm pl}/T) - n_{\rm B}(-\omega_{\rm pl}) \times\exp(-\omega_{\rm pl}/T)] - \sqrt{\frac{\pi}{2}}\frac{T}{2p}\ln(1+\kappa^2p^2/\sigma_p^2). \quad \text{(A8)}$$

At large $p$, the term $\kappa^2p^2/\sigma_p$ dominates the argument of the logarithm, i.e., we can write $\ln(1+\kappa^2p^2/\sigma_p^2)\simeq\ln(\kappa^2p^2/\sigma_p^2)$. Then, we arrive at Eq. (A1), given in Sec. IV.

## APPENDIX B: PADÉ APPROXIMATION

From the knowledge of the behavior of $\sigma_p$ in the limits $p\to0$ and $p\to\infty$, a two-point Padé interpolation formula can be constructed. For the value of the quasiparticle damping width at $p=0$ we take the expression

$$\sigma_0 = -\frac{\pi}{2}\sqrt{\kappa T}, \quad \text{(B1)}$$

which is the exact solution of the self-consistent Born approximation [35].

The Padé interpolation formula is constructed in the following way. We make the ansatz

$$\sigma_p^{\rm Padé} = \frac{a_0+a_1p}{1+b_1p+b_2p^2}\tilde{\varphi}(p), \quad \text{(B2)}$$

where the function $\tilde{\varphi}(p)$ contains the logarithmic terms present in the behavior of $\sigma_p$ at large $p$ [cf. Eq. (16)]:

$$\tilde{\varphi}(p) = \left(\tilde{\xi} - \ln\tilde{\xi} + \frac{\ln\tilde{\xi}}{\tilde{\xi}} - \frac{\ln\tilde{\xi}}{\tilde{\xi}^2} + \frac{\ln\tilde{\xi}}{\tilde{\xi}} - \frac{3\ln^2\tilde{\xi}}{2\tilde{\xi}^3} + \frac{\ln^2\tilde{\xi}}{2\tilde{\xi}^2} + \frac{\ln^3\tilde{\xi}}{3\tilde{\xi}^3}\right), \quad \text{(B3)}$$

$$\tilde{\xi} = \ln\left(e + \sqrt{\frac{2}{\pi}}\kappa p^2\exp(A/T)/T\right). \quad \text{(B4)}$$

The coefficients $a_0,a_1,b_1,b_2$ are determined by power expansion at $p=0$ and $p\to\infty$,

$$\lim_{p\to0}\sigma_p^{\rm Padé} = a_0 + (a_1-a_0b_1)p + O(p^2), \quad \text{(B5)}$$

$$\lim_{p\to\infty}\sigma_p^{\rm Padé} = \left(\frac{a_1}{b_2p} + \frac{a_0b_2-a_1b_1}{b_2^2p^2} + O(p^{-3})\right)\tilde{\varphi}(p), \quad \text{(B6)}$$

and comparison to the behavior of $\sigma_p$ in these limiting cases, e.g., Eq. (16) for large $p$ and Eq. (B1) for $p\to0$. Setting the slope of $\sigma_p$ at $p=0$ to zero, as well as the coefficient in front of the $p^{-2}$ term of the asymptotic expansion, we arrive at the following equations for the coefficients of the interpolation formula:

$$a_0 = -\frac{\pi}{2}\sqrt{\kappa T}, \quad a_1 - a_0b_q = 0, \quad \text{(B7)}$$

$$a_1 = -T\sqrt{\frac{\pi}{2}}b_2, \quad a_0 b_2 - a_1 b_1 = 0. \tag{B8}$$

The solution reads

$$a_0 = -\frac{\pi}{2}\sqrt{\kappa T}, \quad a_1 = -\kappa\left(\frac{\pi}{2}\right)^{3/2}, \tag{B9}$$

$$b_1 = \sqrt{\frac{\pi\kappa}{2T}}, \quad b_2 = \frac{\pi\kappa}{2T}, \tag{B10}$$

which is given as Eq. (17) in the main text, Sec. II.


[1] L. P. Kadanoff and G. Baym, *Quantum Statistical Mechanics* (W. A. Benjamin, New York, 1962).
[2] G. D. Mahan, *Many-Particle Physics*, 2nd ed. (Plenum Press, New York, 1981).
[3] A. L. Fetter and J. D. Walecka, *Quantum Theory of Many-Particle Systems* (McGraw-Hill, New York, 1971).
[4] A. Höll, C. D. Roberts, and S. V. Wright, in *Particles and Fields: X Mexican Workshop*, edited by M. A. Pérez, L. Urrutia, and L. Villaseqor, AIP Conf. Proc. No. 857 (AIP, Melville, NY, 2006), pp. 46–61.
[5] A. Wierling, in *Advances in Plasma Physics Research*, edited by F. Gerard (Nova Science, New York, 2002), p. 127.
[6] H. Reinholz, Ann. Phys. (Paris) **30**, 1 (2005).
[7] C. Fortmann, G. Röpke, and A. Wierling, Contrib. Plasma Phys. **47**, 297 (2007).
[8] H. Reinholz, I. Morozov, G. Röpke, and T. Millat, Phys. Rev. E **69**, 066412 (2004).
[9] D. O. Gericke, M. Schlanges, and W.-D. Kraeft, Phys. Lett. A **222**, 241 (1996).
[10] W.-D. Kraeft and B. Strege, Physica A **149**, 313 (1988).
[11] J. Vorberger, M. Schlanges, and W.-D. Kraeft, Phys. Rev. E **69**, 046407 (2004).
[12] W. D. Kraeft, D. Kremp, W. Ebeling, and G. Röpke, *Quantum Statistics of Charged Particle Systems* (Akademie-Verlag, Berlin, 1986).
[13] W. Ebeling, W.-D. Kraeft, and D. Kremp, *Theory of Bound States and Ionization Equilibrium in Plasmas and Solids* (Akademie-Verlag, Berlin, 1972).
[14] F. J. Dyson, Phys. Rev. **75**, 1736 (1949).
[15] J. Schwinger, Proc. Natl. Acad. Sci. U.S.A. **37**, 451 (1951).
[16] J. Schwinger, Proc. Natl. Acad. Sci. U.S.A. **37**, 455 (1951).
[17] C. D. Roberts and S. M. Schmidt, Prog. Part. Nucl. Phys. **45**, S1 (2000).
[18] L. Hedin, Phys. Rev. **139**, A796 (1965).
[19] U. von Barth, N. E. Dahlen, R. van Leeuwen, and G. Stefanucci, Phys. Rev. B **72**, 235109 (2005).
[20] G. Baym and L. P. Kadanoff, Phys. Rev. **124**, 287 (1961).
[21] G. Baym, Phys. Rev. **127**, 1391 (1962).
[22] F. Aryasetiawan and O. Gunnarsson, Rep. Prog. Phys. **61**, 237 (1998).
[23] G. Onida, L. Reining, and A. Rubio, Rev. Mod. Phys. **74**, 601 (2002).
[24] G. D. Mahan, Comments Condens. Matter Phys. **16**, 333 (1994).
[25] H. van Hees and J. Knoll, Phys. Rev. D **65**, 025010 (2001).
[26] H. van Hees and J. Knoll, Phys. Rev. D **65**, 105005 (2002).
[27] H. van Hees and J. Knoll, Phys. Rev. D **66**, 025028 (2002).
[28] Y. Takada, Phys. Rev. Lett. **87**, 226402 (2001).
[29] U. von Barth and B. Holm, Phys. Rev. B **54**, 8411 (1996).
[30] B. Holm and U. von Barth, Phys. Rev. B **57**, 2108 (1998).
[31] R. Fehr and W.-D. Kraeft, Contrib. Plasma Phys. **35**, 463 (1995).
[32] A. Wierling and G. Röpke, Contrib. Plasma Phys. **38**, 513 (1998).
[33] R. Schepe, T. Schmielau, D. Tamme, and K. Henneberger, Phys. Status Solidi B **206**, 273 (1998).
[34] W. Fennel and H. P. Wilfer, Ann. Phys. (Leipzig) **32**, 265 (1974).
[35] C. Fortmann, J. Phys. A: Math. Theor. **41**, 445501 (2008).
[36] J. N. Bahcall, M. H. Pinsonneault, and G. J. Wasserburg, Rev. Mod. Phys. **67**, 781 (1995).
[37] B. I. Lundquist, Phys. Kondens. Mater. **6**, 206 (1967).
[38] D. Bohm and E. P. Gross, Phys. Rev. **75**, 1851 (1949).
[39] R. Thiele, T. Bornath, C. Fortmann, A. Höll, R. Redmer, H. Reinholz, G. Röpke, A. Wierling, S. H. Glenzer, and G. Gregori, Phys. Rev. E **78**, 026411 (2008).
[40] J. Knoll and D. Voskresensky, Ann. Phys. (N.Y.) **249**, 532 (1996).
[41] A. B. Migdal, Phys. Rev. **103**, 1811 (1956).
[42] S. Klein, Rev. Mod. Phys. **71**, 1501 (1999).
[43] H. D. Hansen, U. I. Uggerhøj, C. Biino, S. Ballestrero, A. Mangiarotti, P. Sona, T. J. Ketel, and Z. Z. Vilakazi, Phys. Rev. Lett. **91**, 014801 (2003).
[44] H. D. Hansen, U. I. Uggerhøj, C. Biino, S. Ballestrero, A. Mangiarotti, P. Sona, T. J. Ketel, and Z. Z. Vilakazi, Phys. Rev. D **69**, 032001 (2004).
[45] C. Fortmann, H. Reinholz, G. Röpke, and A. Wierling, in *Condensed Matter Theory*, edited by J. Clark, R. Panoff, and H. Li (Nova Science, New York, 2005), Vol. 20, p. 317.
[46] *Handbook of Mathematical Functions with Formulas, Graphs and Mathematical Tables*, 9th ed., edited by M. Abramowitz and A. Stegun (Dover Publications, New York, 1970).